

Determined BSS Based on Time-frequency Masking and Its Application to Harmonic Vector Analysis

Kohei Yatabe, *Member, IEEE*, and Daichi Kitamura, *Member, IEEE*

Abstract—When the number of microphones is equal to that of the source signals (the determined situation), audio blind source separation (BSS) is usually performed by multichannel linear filtering to deal with the convolutive mixing process. By formulating the determined BSS problem based on the statistical independence, several methods have been successfully developed. The key to development is the modeling of the source signals, e.g., independent vector analysis (IVA) considers co-occurrence among the frequency components in each source. In this paper, we propose the determined BSS method termed harmonic vector analysis (HVA) by modeling the harmonic structure of audio signals via the sparsity of cepstrum. To handle HVA, the general algorithmic framework that recasts the modeling problem of determined BSS into a design problem of a time-frequency mask is also proposed. Through the experimental investigation, it is shown that HVA outperforms IVA and independent low-rank matrix analysis (ILRMA) for both speech and music signals.

Index Terms—Blind source separation (BSS), independent component analysis (ICA), cepstrum analysis, Wiener-like mask, plug-and-play scheme, proximal splitting algorithm.

I. INTRODUCTION

BLIND source separation (BSS) is methodology of recovering the source signals from multiple mixtures (audio recordings in the case of this paper) without any knowledge about the mixing system. Let a convolutive mixing process of the signals be approximated in the time-frequency domain as

$$\mathbf{x}[t, f] \approx \mathbf{A}[f]\mathbf{s}[t, f], \quad (1)$$

where $\mathbf{x} = [x_1, x_2, \dots, x_M]^T \in \mathbb{C}^M$ is the observed mixtures obtained by M microphones, $\mathbf{s} = [s_1, s_2, \dots, s_N]^T \in \mathbb{C}^N$ is the set of source signals to be recovered, $\mathbf{A}[f] \in \mathbb{C}^{M \times N}$ is the mixing matrix, and t and f are indices of time and frequency, respectively. Then, the aim of BSS is to recover the unknown source signals, \mathbf{s} , only from the mixtures, \mathbf{x} . In the determined ($M = N$) or overdetermined ($M > N$) situation, many of the BSS problems are formulated as an estimation problem of finding (or approximating) a demixing matrix, $\mathbf{W}[f] \in \mathbb{C}^{N \times M}$, that is a left inverse of $\mathbf{A}[f]$ (i.e., $\mathbf{W}[f]\mathbf{A}[f] = \mathbf{I}$, where \mathbf{I} is the identity matrix). Then, the source signals are recovered by the following simple multiplication of the estimated matrix,

$$\mathbf{W}[f]\mathbf{x}[t, f] \approx \mathbf{W}[f]\mathbf{A}[f]\mathbf{s}[t, f] = \mathbf{s}[t, f]. \quad (2)$$

By reducing the BSS problem into the demixing matrix estimation problem, the difficulty of directly tackling the unknown

mixing process in Eq. (1) is circumvented. This paper focuses on the above formulation of the (over)determined BSS, where the demixing matrix $\mathbf{W}[f]$ is estimated for all f only from the observed data $\mathbf{x}[t, f]$ ($t = 1, \dots, T$, $f = 1, \dots, F$).

For estimating the demixing matrix, statistical independence between the source signals is often assumed, which leads to a family of independence-based BSS methods. Arguably, independent component analysis (ICA) [3] applied in the frequency domain (FDICA) [4]–[8] is one of the most famous methods among them. However, FDICA suffers from the permutation problem [9]–[12], and thus some recent development on BSS has aimed to avoid it by introducing more sophisticated models of the source signals. For instance, independent vector analysis (IVA) [13]–[15] assumes co-occurrence among the frequency components in each source, and independent low-rank matrix analysis (ILRMA) [16]–[18] assumes low-rankness on the spectrogram of each source. The key to success of these methods is to incorporate prior knowledge on the source signals into their formulations. That is, improvement brought by these methods relies on the preciseness of their source models. Therefore, seeking a better source model is important for developing a novel and effective BSS method.

However, recent algorithms [18]–[20] cannot handle a new source model directly because they are specialized to each method. These state-of-the-art algorithms are based on the majorization-minimization (MM) principle [21] that requires specially designed upper-bounds of the objective functions. That is, a new algorithm must be derived each time when the source model is modified. Derivation of the upper-bound is usually heuristic, and it might take a lot of time before examining a new source model, especially when the model is a complicated one. If a single algorithm can handle a large number of source models without effort, discovering a better source model should become much easier, and that possibly boosts the development of BSS.

In this paper, to realize such effortless investigation of the source model, we propose a general algorithmic framework based on the implicit source model defined via a time-frequency mask. As the basic principle of the BSS methods is super-Gaussianity, or sparsity, of the source signals in the time-frequency domain, their difference is the way how to impose the sparsity within their separation processes. In this respect, the techniques developed along sparsity-based signal processing [22]–[27], such as the proximal splitting technique [28]–[31], should be beneficial to BSS. Since the optimization problem associated with the independence-based BSS methods (e.g., FDICA, IVA and ILRMA) can be interpreted as the problem comprising the common log-determinant term and a source-model term (see Section II), it can be

The preliminary versions of this work have appeared in the conference proceedings [1], [2] which did not include the harmonic vector analysis.

K. Yatabe is with the Department of Intermedia Art and Science, Waseda University, Tokyo 169-8555, Japan (e-mail: k.yatabe@asagi.waseda.jp).

D. Kitamura is with the Department of Electrical and Computer Engineering, National Institute of Technology, Kagawa College, Kagawa, Japan.

Manuscript received XXXX XX, 20XX; revised XXXX XX, 20XX.

handled through the primal-dual splitting (PDS) algorithm [32] (see Section III). Then, the proximity operator of the PDS algorithm is heuristically extended to a general time-frequency masking method based on the close connection of time-frequency masking to the thresholding operators in sparsity-based signal processing (see Section IV). The resulted algorithm offers tremendous flexibility into determined BSS because any masking method can be utilized to estimate the demixing matrix, even when the corresponding source model cannot be written explicitly.

As an application of the proposed algorithm, we also propose a novel BSS method termed *harmonic vector analysis (HVA)*, which is the main contribution of this paper. To model the source signals, HVA focuses on the harmonic structure of audio signals as a cue for separation. By utilizing sparsity of the cepstrum coefficients, the co-occurrence of the harmonic components is captured. Then, HVA constructs the Wiener-like mask so that the separated signals in each iteration become more exclusive and unmixed. It has the properties of both IVA and ILRMA because HVA can model the spectral pattern as ILRMA while it independently treats each time segment as IVA. Based on the experiments, the proposed HVA can achieve the state-of-the-art performance for both speech and music signals with lower computational cost than ILRMA thanks to the fast Fourier transform (FFT).

The rest of the paper is organized as follows. The estimation problem of the demixing matrices is introduced in Section II together with the connection to the above-mentioned BSS methods. Then, the proximal splitting algorithm is explained in Section III, and its heuristic extension based on time-frequency masking is proposed in Section IV. After HVA is introduced in Section V, they are evaluated experimentally in Section VI. Finally, the paper is concluded in Section VII.

II. INDEPENDENCE-BASED BSS PROBLEM

As introduced in the previous section, BSS methods considered in this paper aim to estimate $N \times M$ demixing matrices, $\{\mathbf{W}[f]\}_{f=1}^F$, that approximately recover the source signals only from the observed mixtures as $\mathbf{W}[f]\mathbf{x}[t, f] \approx \mathbf{s}[t, f]$. To manage this ill-posed problem, the well-accepted assumption is statistical independence between the source signals [33], [34]. While there exist several formulations depending on the method to measure independence, many of them fall into a minimization problem of the following form:

$$\text{Minimize}_{\{\mathbf{W}[f]\}_{f=1}^F} \sum_{n=1}^N \mathcal{P}_n(\mathbf{W}[f]\mathbf{x}[t, f]) - \sum_{f=1}^F \log |\det(\mathbf{W}[f])|, \quad (3)$$

where the log-determinant term is obtained from either maximum likelihood (ML) estimation or minimizing mutual information [33], and \mathcal{P}_n is a real-valued function corresponding to the model of the n th source (in the case of ML estimation, $C \exp(-\mathcal{P}_n(\cdot))$ corresponds to the density function of the n th source). For example, with some constant C , the ℓ_1 norm,

$$\mathcal{P}_n(\mathbf{y}[t, f]) = C \|\mathbf{y}_n[\cdot, \cdot]\|_1 = C \sum_{t=1}^T \sum_{f=1}^F |y_n[t, f]|, \quad (4)$$

recovers FDICA based on the Laplace distribution, and the $\ell_{2,1}$ -mixed norm that treats each time segment as the group,

$$\mathcal{P}_n(\mathbf{y}[t, f]) = C \|\mathbf{y}_n[\cdot, \cdot]\|_{2,1} = C \sum_{t=1}^T \left(\sum_{f=1}^F |y_n[t, f]|^2 \right)^{\frac{1}{2}}, \quad (5)$$

obtains IVA with the spherical Laplace distribution. ILRMA can also be interpreted as Eq. (3) by considering the function that depends on the rank of each spectrogram,

$$\mathcal{P}_n(\mathbf{y}[t, f]) = C \mathcal{D}_R(\mathbf{y}_n[\cdot, \cdot]), \quad (6)$$

where $\mathcal{D}_R(\mathbf{y}_n[\cdot, \cdot])$ is a measure of the low-rankness based on the Itakura–Saito non-negative matrix factorization [35]:

$$\mathcal{D}_R(\mathbf{y}_n[\cdot, \cdot]) = \min_{\varphi_{f,r}^{[n]} \geq 0, \psi_{r,t}^{[n]} \geq 0} \sum_{t=1}^T \sum_{f=1}^F \left(\frac{|y_n[t, f]|^2}{\sum_{r=1}^R \varphi_{f,r}^{[n]} \psi_{r,t}^{[n]}} + \log \sum_{r=1}^R \varphi_{f,r}^{[n]} \psi_{r,t}^{[n]} \right). \quad (7)$$

From this perspective, it is clear that the performance of these methods is determined by the penalty function, \mathcal{P}_n . That is, a BSS method can be improved by finding a better penalty function corresponding to a better source model. For seeking a better model, it is convenient to have a single algorithm that can handle a large number of penalty functions without spending time for its derivation. In this paper, a PDS algorithm is utilized to meet this requirement.

III. PDS ALGORITHM FOR DETERMINED BSS

In this section, a PDS algorithm is applied to the BSS problem in the previous section. The PDS algorithm is briefly reviewed first, and then the BSS problem is reformulated into a PDS applicable form to obtain the proposed algorithm.

A. Primal-dual Splitting (PDS) Algorithm

Let us consider the following minimization problem:

$$\text{Minimize}_{\mathbf{w}} g(\mathbf{w}) + h(\mathbf{L}\mathbf{w}), \quad (8)$$

where g and h are proper lower-semicontinuous convex functions, and \mathbf{L} is a bounded linear operator. Here, both g and h can be non-differentiable, and therefore usual gradient-based optimization methods may not be applicable for solving it. A PDS algorithm [32] is one of the proximal algorithms for solving such problem by iterating the following procedure:

$$\begin{cases} \tilde{\mathbf{w}} = \text{prox}_{\mu_1 g} [\mathbf{w}^{[k]} - \mu_1 \mu_2 \mathbf{L}^* \mathbf{y}^{[k]}], \\ \mathbf{z} = \mathbf{y}^{[k]} + \mathbf{L}(2\tilde{\mathbf{w}} - \mathbf{w}^{[k]}), \\ \tilde{\mathbf{y}} = \mathbf{z} - \text{prox}_{h/\mu_2} [\mathbf{z}], \\ (\mathbf{w}^{[k+1]}, \mathbf{y}^{[k+1]}) = \alpha(\tilde{\mathbf{w}}, \tilde{\mathbf{y}}) + (1 - \alpha)(\mathbf{w}^{[k]}, \mathbf{y}^{[k]}), \end{cases} \quad (9)$$

where \mathbf{L}^* is the adjoint of \mathbf{L} , $\mu_1 > 0$ and $\mu_2 > 0$ are step sizes, and $2 > \alpha > 0$ is a parameter adjusting the speed of convergence ($\alpha = 1$ is the standard speed, while $\alpha > 1$ accelerates and $\alpha < 1$ slows down the algorithm). Note that the last line in Eq. (9) can be omitted when $\alpha = 1$. As the heuristic extension in Section IV will remove the theoretical guarantee of the algorithm, we will not discuss the theoretical

aspects but experimentally show the empirical effectiveness of the algorithm in Section VI. For details and variants of PDS methods, the reader may refer to [32] and references therein.

The important feature of this algorithm is that each function in the problem is minimized via the *proximity operator* [29],

$$\text{prox}_{\mu g}[\mathbf{z}] = \arg \min_{\boldsymbol{\xi}} \left[g(\boldsymbol{\xi}) + \frac{1}{2\mu} \|\mathbf{z} - \boldsymbol{\xi}\|_2^2 \right]. \quad (10)$$

Because this subproblem is easier than the original problem (where the easiness comes from the infimal convolution [30]), the PDS algorithm can handle the difficulty related to the property of the objective functions, such as non-differentiability typical for sparsity-inducing functions, by solving Eq. (10) for g and h separately.

B. Reformulating the Problem into a PDS Applicable Form

To apply the PDS algorithm, the BSS problem in Eq. (3) is reformulated into the PDS applicable form [Eq. (8)]. Firstly, for considering the proximity operator, the second term in Eq. (3) is modified. As the determinant of a matrix can be expressed in terms of its singular values as $|\det(\mathbf{W}[f])| = \prod_{n=1}^N \sigma_n(\mathbf{W}[f])$, Eq. (3) can be rewritten as follows:

$$\text{Minimize}_{\{\mathbf{W}[f]\}_{f=1}^F} \mathcal{P}(\mathbf{W}[f]\mathbf{x}[t, f]) - \sum_{f=1}^F \sum_{n=1}^N \log \sigma_n(\mathbf{W}[f]), \quad (11)$$

where $\sigma_n(\mathbf{W}[f]) \geq 0$ is the n th singular value of $\mathbf{W}[f]$ in descending order. Here, the penalty function, \mathcal{P} , is also slightly generalized by omitting the restriction to a separable function ($\mathcal{P} = \sum_{n=1}^N \mathcal{P}_n$). Note that, while Eq. (3) is defined only for square matrices, this formulation allows rectangular demixing matrices ($N \neq M$). Thus, it does not require dimensionality reduction, typically based on the principal component analysis (PCA), for an over-determined situation, which might be advantageous as discussed in [17].

Next, the optimization variables are vectorized to form a single vector. Let \mathbf{w} be an NMF -dimensional vector corresponding to the demixing matrices, $\{\mathbf{W}[f]\}_{f=1}^F$,

$$\mathbf{w} = [\mathbf{w}[1]^T, \mathbf{w}[2]^T, \dots, \mathbf{w}[F]^T]^T \in \mathbb{C}^{NMF}, \quad (12)$$

$$\mathbf{w}[f] = \text{vec}(\mathbf{W}[f]) \in \mathbb{C}^{NM}, \quad (13)$$

where vec is the vectorizing operator converting a matrix into the corresponding vector in the row-major numbering scheme,

$$\text{vec}(\mathbf{W}[f]) = [W_{1,1}[f], \dots, W_{1,M}[f], W_{2,1}[f], \dots, W_{N,M}[f]]^T, \quad (14)$$

and let mat be the operator converting it back to the matrix,

$$\text{mat}(\mathbf{w})[f] = \mathbf{W}[f], \quad (15)$$

which also indicates that $\mathbf{w}[f] = \text{vec}(\text{mat}(\mathbf{w})[f])$. With these notations, Eq. (11) can be expressed as follows:

$$\text{Minimize}_{\mathbf{w}} \mathcal{P}(\mathbf{X}\mathbf{w}) - \sum_{f=1}^F \sum_{n=1}^N \log \sigma_n(\text{mat}(\mathbf{w})[f]), \quad (16)$$

where \mathbf{X} is an $NTF \times NMF$ sparse matrix constructed by copying the observed data, $\mathbf{x}[t, f]$, as

$$\mathbf{X} = \text{blkdiag}(\chi[1], \chi[2], \dots, \chi[F]) \in \mathbb{C}^{NTF \times NMF}, \quad (17)$$

$$\chi[f] = \text{blkdiag}(\chi[f], \chi[f], \dots, \chi[f]) \in \mathbb{C}^{NT \times NM}, \quad (18)$$

$$\chi[f] = [\tau_1[f], \tau_2[f], \dots, \tau_M[f]] \in \mathbb{C}^{T \times M}, \quad (19)$$

$$\tau_m[f] = [x_m[1, f], x_m[2, f], \dots, x_m[T, f]]^T \in \mathbb{C}^T, \quad (20)$$

and blkdiag is the operator constructing a block-diagonal matrix by concatenating inputted matrices diagonally.

Let the second term in Eq. (16) be shortly denoted by \mathcal{I} :

$$\mathcal{I}(\mathbf{w}) = - \sum_{f=1}^F \sum_{n=1}^N \log \sigma_n(\text{mat}(\mathbf{w})[f]). \quad (21)$$

Then, Eq. (16) can be rewritten in a PDS applicable form:

$$\text{Minimize}_{\mathbf{w}} \mathcal{I}(\mathbf{w}) + \mathcal{P}(\mathbf{X}\mathbf{w}). \quad (22)$$

As the BSS problem is reformulated into this PDS applicable form, the PDS algorithm in Eq. (9) can be applied if the proximity operator of each function is computable.

C. PDS Algorithm for Determined BSS

It is known that the proximity operator of an orthogonally invariant function can be evaluated by applying the corresponding proximity operator to the singular values of the inputted matrix [29]. By regarding $-\log \sigma_n$ in Eq. (21) as $-\log |\sigma_n|$, the proximity operator of $\mathcal{I}(\mathbf{w})$ is obtained [30]:

$$(\text{prox}_{\mu \mathcal{I}}[\mathbf{w}])[f] = \text{vec}(\mathbf{U}[f] \tilde{\Sigma}(\text{mat}(\mathbf{w})[f]) \mathbf{V}[f]^H), \quad (23)$$

where $\mathbf{W}[f] = \mathbf{U}[f] \Sigma[f] \mathbf{V}[f]^H$ is the singular value decomposition of $\mathbf{W}[f]$ ($= \text{mat}(\mathbf{w})[f]$), $\tilde{\Sigma}(\cdot)$ is the diagonal matrix,

$$\tilde{\Sigma}(\mathbf{W}) = \text{diag}(\text{prox}_{-\mu \log}[\sigma_1(\mathbf{W})], \dots, \text{prox}_{-\mu \log}[\sigma_N(\mathbf{W})]), \quad (24)$$

whose diagonal elements comprise the modified singular values calculated by applying the proximity operator of $-\mu \log$,

$$\text{prox}_{-\mu \log}[\sigma] = (\sigma + \sqrt{\sigma^2 + 4\mu})/2, \quad (25)$$

and diag is the operator constructing a diagonal matrix from inputted scalars. In other words, applying the proximity operator of $-\mu \log$ to each singular value of $\mathbf{W}[f]$, for each frequency independently, gives $\text{prox}_{\mu \mathcal{I}}[\cdot]$. It is worth mentioning that this operation is numerically stable because it does not magnify $\|\mathbf{w}\|_2$ much in contrast to the state-of-the-art MM algorithms [18]–[20] which involve inversion of the matrices that sometimes lead to instability.

By using Eq. (23), a PDS algorithm for the BSS problems is obtained as in Algorithm 1. This algorithm can be applied to many BSS models by only changing the 6th line where the proximity operator of the penalty function, $\text{prox}_{\mathcal{P}/\mu_2}[\cdot]$, is computed. Therefore, it can be used to test performance of BSS models without effort on modifying the code whenever the proximity operator of \mathcal{P} is computable. Note that an iterative algorithm can be used to evaluate $\text{prox}_{\mathcal{P}/\mu_2}[\cdot]$ because it is defined by the optimization problem in Eq. (10). That is, it is still possible to apply the proposed algorithm even when the proximity operator does not admit a closed-form solution.

Algorithm 1 PDS-BSS

```

1: Input:  $\mathbf{X}$ ,  $\mathbf{w}^{[1]}$ ,  $\mathbf{y}^{[1]}$ ,  $\mu_1$ ,  $\mu_2$ ,  $\alpha$ 
2: Output:  $\mathbf{w}^{[K+1]}$ 
3: for  $k = 1, \dots, K$  do
4:    $\tilde{\mathbf{w}} = \text{prox}_{\mu_1 \mathcal{I}}[\mathbf{w}^{[k]} - \mu_1 \mu_2 \mathbf{X}^H \mathbf{y}^{[k]}]$ 
5:    $\mathbf{z} = \mathbf{y}^{[k]} + \mathbf{X}(2\tilde{\mathbf{w}} - \mathbf{w}^{[k]})$ 
6:    $\tilde{\mathbf{y}} = \mathbf{z} - \text{prox}_{\frac{1}{\mu_2} \mathcal{P}}[\mathbf{z}]$ 
7:    $\mathbf{y}^{[k+1]} = \alpha \tilde{\mathbf{y}} + (1 - \alpha) \mathbf{y}^{[k]}$ 
8:    $\mathbf{w}^{[k+1]} = \alpha \tilde{\mathbf{w}} + (1 - \alpha) \mathbf{w}^{[k]}$ 
9: end for

```

Some examples of the proximity operators of sparsity-inducing functions that can be written in closed-form will be given in Section IV.

D. PDS Algorithm for Multiple Penalty Functions

A source model consists of two or more penalty functions,

$$\underset{\mathbf{w}}{\text{Minimize}} \quad \mathcal{I}(\mathbf{w}) + \sum_{q=1}^Q \mathcal{P}^{[q]}(\mathbf{X}\mathbf{w}), \quad (26)$$

can also be handled by the PDS algorithm. To deal with this problem, the data matrix, \mathbf{X} , is vertically concatenated as $\mathbf{L} = [\mathbf{X}^T, \dots, \mathbf{X}^T]^T$ (Q times), where \mathbf{L} is the matrix appeared in Eq. (9). Then, the PDS algorithm for Eq. (26) is derived as in Algorithm 2, where $Q = 1$ reduces to Algorithm 1. As presented in the algorithm, each penalty function $\mathcal{P}^{[q]}$ is independently handled by the corresponding proximity operator. Thus, a complicated BSS model decomposable into several simple functions $\{\mathcal{P}^{[q]}\}_{q=1}^Q$ can be handled easily. Examples of such models may include the group-sparse model of harmonic/percussive source separation [36] and the sparse and low-rank model of robust PCA [37], [38].

Note that, because the product $\mathbf{X}(2\tilde{\mathbf{w}} - \mathbf{w}^{[k]})$ in the 6th line of Algorithm 2 can be calculated outside the loop of q , the number of matrix-vector multiplication is independent of the number of the penalty functions, Q . Therefore, the overall computational cost does not increase much by adding a new penalty function as long as the corresponding proximity operator can be calculated cheaply, which is a usual situation for a sparsity-inducing penalty. Also note that the matrix-vector product by \mathbf{X} (and by \mathbf{X}^H) can be implemented without explicitly constructing the matrix \mathbf{X} , which can reduce the computational requirement.

E. Data Normalization for a Simple Choice of Parameters

The step-size parameters in the PDS algorithm, μ_1 and μ_2 , must be chosen carefully so that the algorithm properly works. When the problem is convex as in Section III-A, a set of parameters for guaranteed convergence is given by [32]

$$\mu_1 \mu_2 \|\mathbf{L}\|_s^2 \leq 1, \quad (27)$$

where $\|\cdot\|_s$ denotes the spectral norm ($\|\mathbf{L}\|_s = \sigma_1(\mathbf{L})$), $\mathbf{L} = \mathbf{X}$ for Algorithm 1, and $\mathbf{L} = [\mathbf{X}^T, \dots, \mathbf{X}^T]^T$ (Q times) for Algorithm 2. Unfortunately, the BSS problem is not convex, even when \mathcal{P} is convex, owing to the $-\log \sigma_n$ term, and

Algorithm 2 PDS-BSS-multiPenalty

```

1: Input:  $\mathbf{X}$ ,  $\mathbf{w}^{[1]}$ ,  $\mathbf{y}_1^{[1]}, \dots, \mathbf{y}_Q^{[1]}$ ,  $\mu_1$ ,  $\mu_2$ ,  $\alpha$ 
2: Output:  $\mathbf{w}^{[K+1]}$ 
3: for  $k = 1, \dots, K$  do
4:    $\tilde{\mathbf{w}} = \text{prox}_{\mu_1 \mathcal{I}}[\mathbf{w}^{[k]} - \mu_1 \mu_2 \mathbf{X}^H (\sum_{q=1}^Q \mathbf{y}_q^{[k]})]$ 
5:   for  $q = 1, \dots, Q$  do
6:      $\mathbf{z}_q = \mathbf{y}_q^{[k]} + \mathbf{X}(2\tilde{\mathbf{w}} - \mathbf{w}^{[k]})$ 
7:      $\tilde{\mathbf{y}}_q = \mathbf{z}_q - \text{prox}_{\frac{1}{\mu_2} \mathcal{P}_q}[\mathbf{z}_q]$ 
8:      $\mathbf{y}_q^{[k+1]} = \alpha \tilde{\mathbf{y}}_q + (1 - \alpha) \mathbf{y}_q^{[k]}$ 
9:   end for
10:   $\mathbf{w}^{[k+1]} = \alpha \tilde{\mathbf{w}} + (1 - \alpha) \mathbf{w}^{[k]}$ 
11: end for

```

thus the above choice of the parameters cannot guarantee the convergence without some additional investigation. Nevertheless, this choice of step sizes, derived for convex problems, seems working as later shown by the experimental results¹. Therefore, in this paper, we follow the above rule for setting the parameters.

By calculating the value of $\|\mathbf{L}\|_s^2$ (which can be efficiently computed by an iterative algorithm, e.g., the power method), the criterion in Eq. (27) can be utilized. To make the choice of the parameters simpler, we propose the following normalization rule of the data matrix, \mathbf{X} :

$$\tilde{\mathbf{X}} = \mathbf{X} / (\sqrt{Q} \|\mathbf{X}\|_s). \quad (28)$$

This normalization results in $\|\mathbf{L}\|_s = 1$, and therefore it allows the following simple choice of the step-size parameters,

$$\mu_1 = 1, \quad \mu_2 = 1. \quad (29)$$

Remind that α can be arbitrarily chosen from $(0, 2)$ [32] or chosen as 1 which bypasses the last line of Eq. (9). Thus, with this normalization, there is nothing to worry about in regards to the choice of the parameters of the PDS algorithms. Their appropriateness will be shown in the experimental section.

IV. GENERAL TIME-FREQUENCY MASKING AS A HEURISTIC SUBSTITUTE OF THE PROXIMITY OPERATOR

In this section, some examples of the proximity operators are introduced as the thresholding functions which can be used in the PDS algorithms. Then, we connect them with the time-frequency masks to interpret the PDS algorithm as an iterative masking procedure. This reinterpretation opens a door to a new possibilities of the BSS algorithms.

¹ Such empirical convergence might be because of the nature of the non-convexity of $-\log \sigma_n$. Note that the BSS problem becomes convex when all $\mathbf{W}[f]$ are restricted to symmetric positive semi-definite (and, of course, when \mathcal{P} is convex). That is, the non-convexity of $-\log \sigma_n$ results in phase ambiguity of the eigenvalues of \mathbf{W} when it is a square matrix. Such ambiguity (together with the scale and permutation ambiguities) in the separated result is usually treated by the post-processing [39]. Therefore, it could be expected that the effect of the non-convexity is canceled out by the post-processing when \mathcal{P} is convex. Although some experimental data suggested that this expectation could be true, an additional analysis is required for understanding the effect of the non-convexity of $-\log \sigma_n$ in terms of BSS.

A. Thresholding Functions Related to the Proximity Operators

As well-known, the proximity operators of several sparsity-inducing penalty functions can be computed analytically. For example, the proximity operator associated with the ℓ_1 norm in Eq. (4) is given by the bin-wise soft-thresholding operator,

$$(\text{prox}_{\lambda \|\cdot\|_1}[\mathbf{z}])_n[t, f] = \left(1 - \frac{\lambda}{|z_n[t, f]|}\right)_+ z_n[t, f], \quad (30)$$

where $\lambda \geq 0$, and $(\cdot)_+ = \max\{0, \cdot\}$ is the half-wave rectifier replacing negative values by zero. That of the $\ell_{2,1}$ -mixed norm in Eq. (5) is also given by the group-thresholding operator,

$$(\text{prox}_{\lambda \|\cdot\|_{2,1}}[\mathbf{z}])_n[t, f] = \left(1 - \frac{\lambda}{(\sum_{f=1}^F |z_n[t, f]|^2)^{\frac{1}{2}}}\right)_+ z_n[t, f]. \quad (31)$$

By inserting one of these proximity operators into the 6th line of Algorithm 1, the PDS algorithm for FDICA or IVA is obtained. Proximity operators associated with many other sparsity-inducing functions can also be computed as thresholding operators [22]. While the penalty functions in the above examples are all convex, the proximity operator is also well-defined for some non-convex functions [27] which induces sparsity more strongly than the convex ones.

By adding the $\ell_{2,1}$ -mixed norm and the ℓ_1 norm, a new BSS model, the sparsely regularized IVA, can be obtained [1]. The PDS algorithm can handle such a new model by just inserting

$$\text{prox}_{\lambda_1 \|\cdot\|_{2,1} + \lambda_2 \|\cdot\|_1}[\mathbf{z}] = \text{prox}_{\lambda_1 \|\cdot\|_{2,1}}[\text{prox}_{\lambda_2 \|\cdot\|_1}[\mathbf{z}]] \quad (32)$$

to the 6th line of Algorithm 1 [40]. However, in general, a proximity operator of sum of multiple functions is difficult to compute even when the proximity operator for each function is simple. Indeed, decomposition as in Eq. (32) is allowed only for a combination of the functions belonging to a specific class of penalty functions [41]–[43]. Therefore, Algorithm 2 was proposed so that multiple proximity operators can be combined without effort. New BSS methods can be systematically generated from a combination of known proximity operators [28]–[30] by inserting them into Algorithm 2.

B. Generalized Thresholding Operators

The generalized thresholding is an interesting trend in sparse signal processing. While the thresholding functions in the previous subsection were obtained from the corresponding penalty functions, the $\ell_{2,1}$ -mixed and ℓ_1 norms, it is possible to define a thresholding operator without defining the penalty function. Some recent research considers this way to realize a better thresholding function [44]–[48]. For example, the thresholding rule obtained through the p -shrinkage [45],

$$(\mathcal{T}_p^\lambda[\mathbf{z}])_n[t, f] = \left(1 - \frac{\lambda^{2-p}}{|z_n[t, f]|^{2-p}}\right)_+ z_n[t, f], \quad (33)$$

corresponds to a penalty function which does not have an explicit formula for general p . Nevertheless, it behaves as a reasonable thresholding function since $p = 1$ results in the soft-thresholding in Eq. (30), and $p \rightarrow -\infty$ corresponds to the hard-thresholding. Note that, although this interpolating nature between soft- and hard-thresholding resembles ℓ_p quasinorm

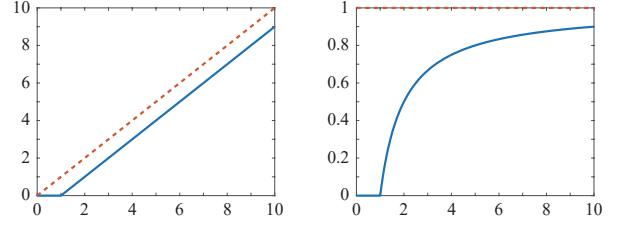


Fig. 1. Soft-thresholding and its mask. The soft-thresholding shown on the left (solid line) corresponds to the mask in Eq. (36) shown on the right.

($0 < p < 1$) which is a popular non-convex sparsity-inducing function, its proximity operator is analytically computable for only few choices of p (e.g., $p = 1/2$ and $p = 2/3$) in contrast to Eq. (33) which is available for all $p \leq 1$.

Another example is one of the social sparsity operators [44],

$$(\mathcal{T}_h^\lambda[\mathbf{z}])_n[t, f] = \left(1 - \frac{\lambda}{(h * |z_n[t, f]|^2)^{\frac{1}{2}}}\right)_+ z_n[t, f], \quad (34)$$

where $h*$ represents the convolution with a two-dimensional filter kernel h , whose elements are non-negative, in the time-frequency domain. Although Eq. (34) is not a proximity operator in general, its effectiveness was empirically shown in [44]. In practice, one can insert any thresholding-like function into Algorithm 1 and 2 to generate a new BSS algorithm.

C. Interpretation of Thresholding as Time-Frequency Masking

Obviously, the above thresholding functions in Eqs. (30)–(34) can be represented by the following single formula,

$$(\mathcal{T}^\lambda[\mathbf{z}])_n[t, f] = (\mathcal{M}(\mathbf{z}))_n[t, f] z_n[t, f], \quad (35)$$

where $0 \leq (\mathcal{M}(\mathbf{z}))_n[t, f] \leq 1$ is a non-negative real scalar depending on the input \mathbf{z} . This can be seen as time-frequency masking with a data-dependent mask $\mathcal{M}(\mathbf{z})$. For instance, the mask corresponding to the soft-thresholding in Eq. (30) is

$$(\mathcal{M}_{\ell_1}^\lambda(\mathbf{z}))_n[t, f] = \left(1 - \frac{\lambda}{|z_n[t, f]|}\right)_+, \quad (36)$$

as in Fig. 1, and that of the group-thresholding in Eq. (31) is

$$(\mathcal{M}_{\ell_{2,1}}^\lambda(\mathbf{z}))_n[t, f] = \left(1 - \frac{\lambda}{(\sum_{f=1}^F |z_n[t, f]|^2)^{\frac{1}{2}}}\right)_+. \quad (37)$$

Based on this observation, Algorithm 2 is rewritten as in Algorithm 3, where \odot denotes the element-wise product, and θ represents a set of parameters for generating the mask.

This slight generalization of the algorithm opens up a new frontier because, as in the previous subsection, any rule for constructing the mask can be combined into the algorithm. That is, any thresholding function and/or sound enhancement method based on time-frequency masking can collaborate with determined BSS through the proposed algorithm. Although stability and convergence of the algorithm for a general time-frequency mask can only be investigated by experiments, testing the ability of the collaboration is easy since the only effort for rewriting the code is in the 7th line of Algorithm 3. Therefore, one can just insert a masking method into the algorithm and run it for checking the performance.

Algorithm 3 PDS-BSS-masking

```

1: Input:  $\mathbf{X}$ ,  $\mathbf{w}^{[1]}$ ,  $\mathbf{y}_1^{[1]}, \dots, \mathbf{y}_Q^{[1]}$ ,  $\mu_1, \mu_2, \alpha$ 
2: Output:  $\mathbf{w}^{[K+1]}$ 
3: for  $k = 1, \dots, K$  do
4:    $\tilde{\mathbf{w}} = \text{prox}_{\mu_1 \mathcal{I}}[\mathbf{w}^{[k]} - \mu_1 \mu_2 \mathbf{X}^H (\sum_{q=1}^Q \mathbf{y}_q^{[k]})]$ 
5:   for  $q = 1, \dots, Q$  do
6:      $\mathbf{z}_q = \mathbf{y}_q^{[k]} + \mathbf{X}(2\tilde{\mathbf{w}} - \mathbf{w}^{[k]})$ 
7:      $\tilde{\mathbf{y}}_q = \mathbf{z}_q - \mathcal{M}_q^\theta(\mathbf{z}_q) \odot \mathbf{z}_q$ 
8:      $\mathbf{y}_q^{[k+1]} = \alpha \tilde{\mathbf{y}}_q + (1 - \alpha) \mathbf{y}_q^{[k]}$ 
9:   end for
10:   $\mathbf{w}^{[k+1]} = \alpha \tilde{\mathbf{w}} + (1 - \alpha) \mathbf{w}^{[k]}$ 
11: end for

```

D. Time-Frequency Masking as MAP Estimation

The above heuristic generalization of the proposed algorithm is closely related to the plug-and-play scheme [49]. Its concept is based on the interpretation of the proximity operator as a maximum *a posteriori* (MAP) estimation. By interpreting the definition of the proximity operator in Eq. (10) as the negative log-likelihood, it can be viewed as the MAP estimator for the observation contaminated by the additive Gaussian noise with a prior distribution $C \exp(-\mathcal{P}(\cdot))$:

$$\text{prox}_{\lambda \mathcal{P}}[\mathbf{z}] = \arg \max_{\boldsymbol{\xi}} \left[e^{-\frac{1}{2\lambda} \|\mathbf{z} - \boldsymbol{\xi}\|_2^2} e^{-\mathcal{P}(\boldsymbol{\xi})} \right]. \quad (38)$$

This interpretation suggests that substituting a general Gaussian denoiser, which approximately solves Eq. (38), in place of the proximity operator results in an algorithm that works as if the function \mathcal{P} is minimized. Such substitution greatly extend the possibility of proximal algorithms because many Gaussian denoisers, which are directly defined as a procedure or learned from data, do not admit an explicit formula for the corresponding \mathcal{P} .

When the underlying penalty function is separable for each source as in Section II ($\mathcal{P} = \sum_{n=1}^N \mathcal{P}_n$), then the proposed algorithm can be seen as an independence-based BSS method (ML estimation) with $C \exp(-\mathcal{P}_n(\cdot))$ being the density function of the n th source signal. That is, the proposed algorithm recasts the BSS problem into the denoising problem in Eq. (38) consisting of the same prior distribution of the sources. This is important property for a data-driven strategy because learning a Gaussian denoiser is much easier than learning a regressor of the demixing matrix which requires a variety of impulse responses as the data. One can insert a source enhancement method, based on time-frequency masking, into Algorithm 3 and obtain a new BSS algorithm.

It is also possible to obtain a BSS algorithm beyond the independence-based framework, at least as a procedure, by inserting a masking method which is not separable for each source signal. We propose such non-separable mask in the next section and demonstrate its effectiveness in the later section.

E. Relation to the Model-based IVA

Here, relation between the proposed method and the model-based IVA [50] is discussed. The model-based IVA is an extension of IVA that utilizes a single-channel enhancement method

to construct the source model. By considering the time-frequency-variant Gaussian distribution as the source model, with variance $v_n[t, f]$, the penalty function corresponding to the model-based IVA can be written as a weighted ℓ_2 norm,

$$\mathcal{P}_n(\mathbf{y}[t, f]) = C \|\mathbf{y}_n[\cdot, \cdot]\|_{2, \mathbf{v}}^2 = C \sum_{t=1}^T \sum_{f=1}^F \frac{|y_n[t, f]|^2}{v_n[t, f]}, \quad (39)$$

which penalizes a time-frequency bin with small variance more than that with large variance. A single-channel source enhancement method (spectral subtraction in the case of [50]) is utilized to set the variance as $v_n[t, f] = |\hat{x}_n[t, f]|^2$, where $\hat{x}_n[t, f]$ is an enhanced version of the observed signal.

As its proximity operator is a shrinkage operator given by

$$(\text{prox}_{\frac{\lambda}{2} \|\cdot\|_{2, \mathbf{v}}^2}[\mathbf{z}])_n[t, f] = \left(\frac{v_n[t, f]}{v_n[t, f] + \lambda} \right) z_n[t, f], \quad (40)$$

the model-based IVA can also be handled by the proposed algorithm via the mask, $(\mathcal{M}(\mathbf{z}))_n[t, f] = v_n[t, f]/(v_n[t, f] + \lambda)$, which is independent of the inputted variable \mathbf{z} (i.e., constant for every iteration). Although the two methods are related in terms of using a general time-frequency masking method for estimating the demixing matrix, the model-based IVA utilizes the mask only once, before starting iteration, to calculate the weight, $v_n[t, f] = |(\mathcal{M}(\mathbf{x}))_n[t, f] x_n[t, f]|^2$, while the proposed algorithm uses the mask within the iteration by updating it based on the inputted variable at that time. That is, the model-based IVA can be seen as the special case of the proposed masking-based BSS framework.

V. HARMONIC VECTOR ANALYSIS (HVA): A NOVEL BSS METHOD BASED ON THE HARMONIC STRUCTURE

As an application of the proposed algorithm, a BSS method named HVA is proposed in this section. It generates the mask based on the cepstrum thresholding that enhances the harmonic structure of the signals. While it might be more natural to consider a recent source enhancement method (such as deep-learning-based one) for the mask as discussed in Section IV-D, our motivation of proposing HVA is to show that there is still a large room for improving hand-crafted BSS models, and the proposed concept in Section IV is essential for that. As HVA is computationally cheaper than many recent methods including ILRMA, it should be suitable for resource-limited devices.

A. Harmonic Structure of Audio Signals

In HVA, the harmonic structure is considered as the basis of the mask generation. As an illustrative example, a log-amplitude spectrum of a voiced segment of a speech signal is shown on the left side of Fig. 2(a). The periodic repetition of the peaks and dips is called harmonic structure and is typical of real-world audio signals. This co-occurrence of the harmonic components should be useful for resolving the permutation problem and separating the source signals. To incorporate this prior knowledge into BSS, a time-frequency mask enhancing the repetitive structure is designed and inserted into the proposed algorithm in the previous section.

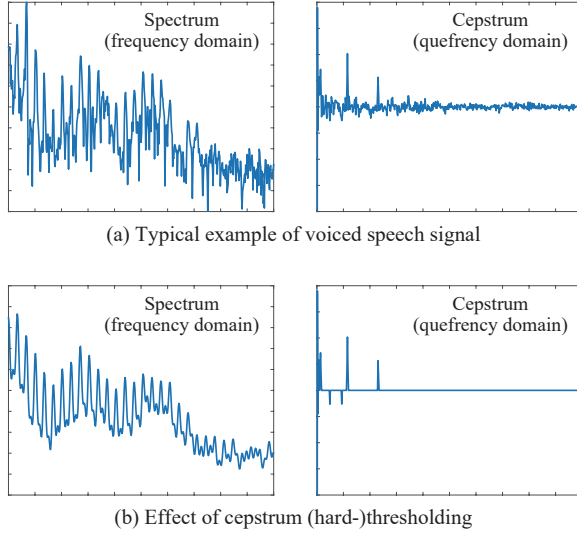


Fig. 2. Typical example of a voiced speech signal and its enhanced version. (a) Log-amplitude spectrum of a segment of voiced speech and its cepstrum coefficients. (b) Result of the hard-thresholding on the cepstrum coefficients that enhances the harmonic structure as in Section V-B.

B. Cepstrum Thresholding Enhancing the Harmonic Structure

One of the well-accepted concepts related to the harmonic structure is *cepstrum*. Since the log-amplitude spectrum is periodic, it can be well-approximated by a few Fourier-series coefficients if it exhibits the harmonic structure. To capture such property, cepstrum is defined as the Fourier transform of a log-amplitude spectrum. By denoting the element-wise absolute value as $(\text{abs}(\mathbf{z}))_n[t, f] = |z_n[t, f]|$, cepstrum of a spectrogram for all segments and channels can be written as

$$(\text{cep}(\mathbf{z}))_n[t, c] = (\mathcal{F}_f(\log(\text{abs}(\mathbf{z}))))_n[t, c], \quad (41)$$

where $\log(\cdot)$ is the element-wise logarithmic function, and \mathcal{F}_f is the frequency-directional Fourier transform,

$$(\mathcal{F}_f(\mathbf{z}))_n[t, c] = \frac{1}{\sqrt{F}} \sum_{f=1}^F z_n[t, f] e^{-2\pi i(c-1)(f-1)/F}. \quad (42)$$

By introducing a Fourier thresholding operator $\mathcal{T}_{\mathcal{F}}^{\lambda}$ with some sparsity-promoting thresholding operator $\mathcal{T}_{\text{sp}}^{\lambda}$ as

$$\mathcal{T}_{\mathcal{F}}^{\lambda}(\mathbf{z}) = \mathcal{F}_f^{-1}(\mathcal{T}_{\text{sp}}^{\lambda}(\mathcal{F}_f(\mathbf{z}))), \quad (43)$$

we define *cepstrum thresholding* that applies the sparsity-inducing thresholding in the cepstrum domain:

$$\mathcal{T}_{\text{cep}}^{\lambda}(\mathbf{z}) = \exp(\mathcal{T}_{\mathcal{F}}^{\lambda}(\log(\text{abs}(\mathbf{z})))), \quad (44)$$

where $\exp(\cdot)$ is the element-wise exponential function, and \mathcal{F}_f^{-1} is the frequency-directional inverse Fourier transform,

$$(\mathcal{F}_f^{-1}(\mathbf{z}))_n[t, f] = \frac{1}{\sqrt{F}} \sum_{c=1}^F z_n[t, c] e^{2\pi i(c-1)(f-1)/F}. \quad (45)$$

The effect of this thresholding is demonstrated in Fig. 2. The cepstrum of the log-amplitude spectrum in Fig. 2(a) contains larger peaks corresponding to the harmonic structure. As the cepstrum thresholding removes small cepstrum coefficients and retain larger coefficients, it enhances the harmonic structure as on the left side of Fig. 2(b).

Algorithm 4 Harmonic Vector Analysis (HVA)

```

1: Input:  $\mathbf{X}, \mathbf{w}^{[1]}, \mathbf{y}^{[1]}, \mu_1, \mu_2, \alpha$ 
2: Output:  $\mathbf{w}^{[K+1]}$ 
3: for  $k = 1, \dots, K$  do
4:    $\tilde{\mathbf{w}} = \text{prox}_{\mu_1 \mathcal{I}}[\mathbf{w}^{[k]} - \mu_1 \mu_2 \mathbf{X}^H \mathbf{y}^{[k]}]$ 
5:    $\mathbf{z} = \mathbf{y}^{[k]} + \mathbf{X}(2\tilde{\mathbf{w}} - \mathbf{w}^{[k]})$ 
6:    $\tilde{\mathbf{y}} = \mathbf{z} - \mathcal{M}_{\text{HVA}}^{\lambda, \sigma}(\mathbf{z}) \odot \mathbf{z}$ 
7:    $\mathbf{y}^{[k+1]} = \alpha \tilde{\mathbf{y}} + (1 - \alpha) \mathbf{y}^{[k]}$ 
8:    $\mathbf{w}^{[k+1]} = \alpha \tilde{\mathbf{w}} + (1 - \alpha) \mathbf{w}^{[k]}$ 
9: end for

```

C. Non-separable Masking for Source Separation

To utilize the prior knowledge in the proposed algorithm, it must be expressed in terms of masking. While the independence criterion has forced ordinary BSS methods to be a procedure separable for each source signal, it is also possible to define a non-separable BSS method handling all source signals simultaneously. The proposed algorithm can realize such method through a non-separable mask-generating function: for example, the Wiener-like mask [51], [52],

$$(\mathcal{M}_{\text{WL}}(\hat{\mathbf{x}}))_n[t, f] = \left(\frac{|\hat{x}_n[t, f]|^2}{\sum_{n=1}^N |\hat{x}_n[t, f]|^2} \right)^{\gamma}, \quad (46)$$

where \hat{x}_n is the enhanced spectrogram corresponding to the n th source signal, and $\gamma > 0$. It should be more effective for promoting source separation than separable masks because it encourages each bin to be more exclusive and unmixed.

Note that, when $\gamma = 1$, this mask can be viewed as a non-separable version of the mask in Eq. (40) related to the time-frequency-variant Gaussian model, where the constant λ in the denominator is replaced by sum of the other source signals.

D. Harmonic Vector Analysis (HVA)

By combining the cepstrum thresholding and Wiener-like masking in the previous subsections, we propose HVA via the following mask inserted in the proposed algorithm:

$$(\mathcal{M}_{\text{HVA}}^{\lambda, \sigma}(\mathbf{z}))_n[t, f] = \left(\frac{v_n^{\mathbf{z}, \lambda, \sigma, \varepsilon}[t, f]}{\sum_{n=1}^N v_n^{\mathbf{z}, \lambda, \sigma, \varepsilon}[t, f]} \right)^{\gamma}, \quad (47)$$

where $v_n^{\mathbf{z}, \lambda, \sigma, \varepsilon}[t, f] = \exp(2\varrho_n^{\mathbf{z}, \lambda, \sigma, \varepsilon}[t, f])$ is the squared amplitude spectrograms whose harmonic structures are enhanced by the cepstrum thresholding, $\varrho_n^{\mathbf{z}, \lambda, \sigma, \varepsilon}[t, f]$ is its logarithm,

$$\varrho_n^{\mathbf{z}, \lambda, \sigma, \varepsilon}[t, f] = (\mathcal{T}_{\mathcal{F}}^{\lambda, \sigma}(\rho^{\mathbf{z}, \varepsilon}))_n[t, f] + \mu_n^{\mathbf{z}, \varepsilon}[t, f], \quad (48)$$

$\rho^{\mathbf{z}, \varepsilon}$ is mean-subtracted log-amplitude spectrograms,

$$\rho_n^{\mathbf{z}, \varepsilon}[t, f] = \log(|z_n[t, f]| + \varepsilon) - \mu_n^{\mathbf{z}, \varepsilon}[t, f], \quad (49)$$

$\mu_n^{\mathbf{z}, \varepsilon}[t] = (1/F) \sum_{f=1}^F \log(|z_n[t, f]| + \varepsilon)$ is the mean value of the log-amplitude spectrum, $\mathcal{T}_{\mathcal{F}}^{\lambda, \sigma}$ is the thresholder in Eq. (43), and ε is a small constant for preventing $\rho_n^{\mathbf{z}, \varepsilon}[t, f]$ to be $-\infty$. The subtraction and addition of the mean value, $\mu_n^{\mathbf{z}, \varepsilon}[t, f]$, within the cepstrum thresholding are performed so that the energy of the squared amplitude spectrograms, $v_n^{\mathbf{z}, \lambda, \sigma, \varepsilon}[t, f]$, remains similar to that of the input spectrogram, \mathbf{z} . The proposed algorithm for HVA is shown in Algorithm 4.

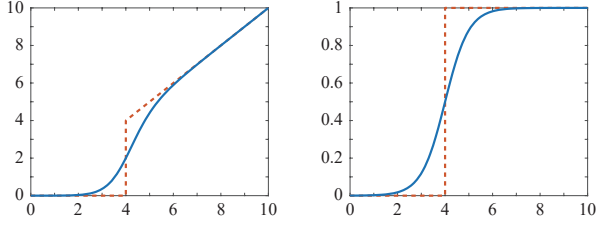


Fig. 3. Smoothed hard-thresholding and its mask for $\lambda = 4$ and $\sigma = 0.5$. The smoothed hard-thresholding in Eq. (50) (solid line) is shown on the left with the usual hard-thresholding (dashed line). The corresponding masks (the sigmoid and step functions) are shown on the right.

To reduce the number of parameters, ε is omitted from $\mathcal{M}_{\text{HVA}}^{\lambda, \sigma}$ because its effect to the performance is not significant (ε is fixed to 10^{-3} in the rest of the paper). We also fixed γ to $1/N$ because of the following reason. When $v_n^{\mathbf{z}, \lambda, \sigma, \varepsilon}[t, f]$ is the same for all n , the value inside the parentheses of Eq. (47) is $1/N$, which depends on N . By setting $\gamma = 1/N$, the value of the mask for that case becomes $(1/N)^{(1/N)} \approx 0.7$ that is approximately independent of N . The other two parameters, λ and σ , should be chosen based on the magnitude of the cepstrum coefficients of the observed signals.

For \mathcal{T}_{sp} in Eq. (43), any sparsity-promoting operator can be adopted. In this paper, the smoothed hard-thresholding [53],

$$(\mathcal{T}_{\text{sp}}^{\lambda, \sigma}(\mathbf{z}))_n[t, c] = \frac{z_n[t, c]}{1 + e^{-(|z_n[t, c]| - \lambda)/\sigma}}, \quad (50)$$

is utilized because it shrinks smaller coefficients without bias on larger coefficients. Note that this thresholding operator can be written as $\text{sigmoid}(\text{abs}(\mathbf{z})) \odot \mathbf{z}$, where $\text{sigmoid}(\cdot)$ is the element-wise sigmoid function. Its graph is illustrated in Fig. 3 together with the hard-thresholding without smoothing.

VI. EXPERIMENTS

In this paper, we proposed the general BSS algorithm and its specific application termed HVA. For illustrating the properties of both algorithm and HVA, some experiments are conducted in this section. At first, the properties of the algorithm and HVA are investigated using two 2-channel speech mixtures as examples. Then, the performances of HVA over speech and music mixtures in 2- and 3-channel conditions are compared with IVA and ILRMA to show its effectiveness.

A. Basic Properties of the Proposed Algorithm

The proposed algorithms contain three parameters μ_1 , μ_2 , and α . Their effects to the performance are investigated using the well-understood IVA. The database used in this experiment was a part of SiSEC [54] (dev1 in the underdetermined audio source separation task). Live recording (liverec) of four female speech sources recorded by two microphones was chosen as the test data. For making the problem determined, two pairs of sources were considered as in Fig. 4. The reverberation time was 130 ms, and the half-overlapping 2048-points-long Hann window (128 ms) was used for the short-time Fourier transform (STFT). The initial value of the demixing matrices $\mathbf{w}^{[1]}$ was set to the identity matrices ($\mathbf{W}[f] = \mathbf{I}$ for all f), and

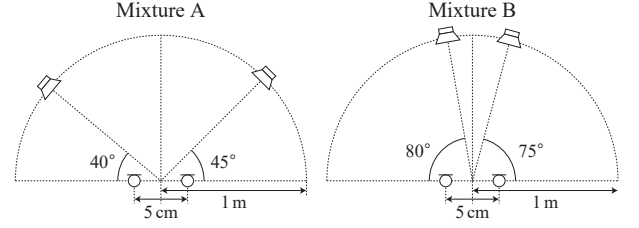


Fig. 4. Recording conditions of the 2-channel speech mixtures utilized in the experiments in Sections VI-A and VI-B using the Laplace IVA.

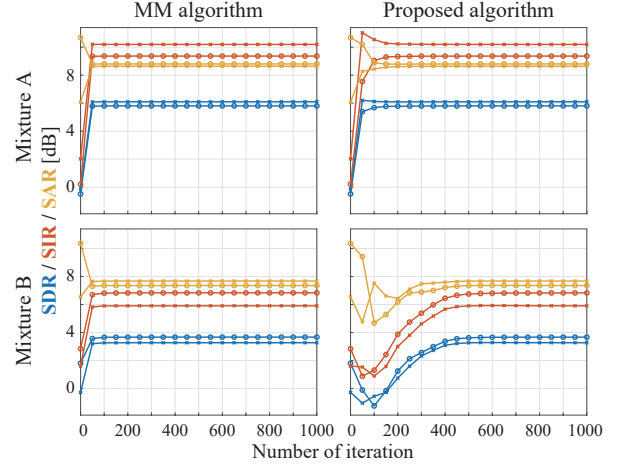


Fig. 5. SDR/SIR/SAR of the separated signals from the mixtures in Fig. 4. The two sources in each mixture are distinguished by the markers (\circ and \times).

that of \mathbf{y} was the zero vector. The BSS method tested here was IVA based on the spherical Laplace distribution, $\mathcal{P}_n = \|\cdot\|_{2,1}$ in Eq. (5), whose proximity operator is given in Eq. (31).

Before investigating the effects of parameters, the proposed algorithm was compared with the MM algorithm based on the iterative projection technique (auxIVA [20]) to confirm that the Laplace IVA was appropriately realized by the proposed algorithm. Their performances over iteration are shown in Fig. 5, where the parameters were set to $\mu_1 = \mu_2 = 1$, and $\alpha = 1.75$. From the figure, it can be seen that the proposed algorithm resulted in the same scores, which indicates that the proposed algorithm was properly working, but required more iterations than the MM algorithm. Note that the computation per iteration of the proposed algorithm was 1.7 times faster than the MM algorithm.

1) *Effect of the Relaxation Parameter α* : As mentioned in Section III-A, the parameter α can speed up ($2 > \alpha > 1$) or slow down ($1 > \alpha > 0$) the convergence of the algorithm. To illustrate such effect, the performances for different $\alpha \in \{0.5, 1, 1.5\}$ were investigated as shown in Fig. 6, where the other parameters were set to $\mu_1 = \mu_2 = 1$. As expected, higher α achieved the final scores with less iterations (note that the case for $\alpha = 1.75$ is shown in Fig. 5).

2) *Effect of the Step-size Parameters μ_1 and μ_2* : As discussed in Section III-E, the data normalization allows the choice $\mu_1 \mu_2 = 1$ for the step size, which comes from Eq. (27). Because μ_1 and μ_2 balance the effects of the proximity

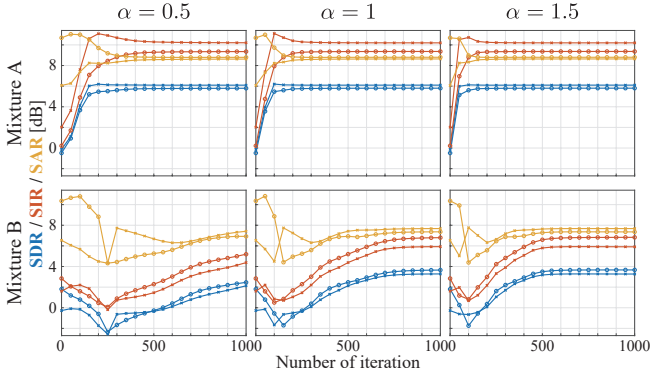


Fig. 6. SDR/SIR/SAR of the separated signals from the mixtures in Fig. 4, where the parameter α was varied (Section VI-A1).

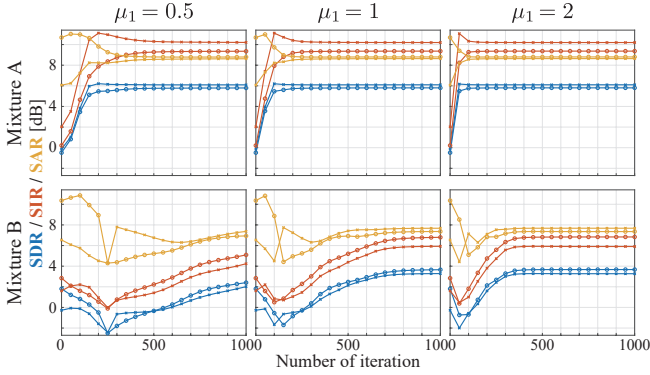


Fig. 7. SDR/SIR/SAR of the separated signals from the mixtures in Fig. 4, where the parameter μ_1 was varied and $\mu_2 = 1/\mu_1$ (Section VI-A2).

operators ($\text{prox}_{\mu_1 \mathcal{I}}$ and $\text{prox}_{\mathcal{P}/\mu_2}$ in Algorithm 1), their choice can also affect the convergence. By setting $\mu_2 = 1/\mu_1$ and $\alpha = 1$, the performances of the proposed algorithm were investigated for $\mu_1 \in \{0.5, 1, 2\}$ as illustrated in Fig. 7. From Figs. 6 and 7, it can be said that a specific choice of the parameters (μ_1 , μ_2 and α) does not have a significant impact on the separation performance for the Laplace IVA if the number of iterations is sufficiently large. This result should be because the penalty function of the Laplace IVA (the $\ell_{2,1}$ mixed norm) is a convex function, and the corresponding proximity operator is theoretically obtained.

B. Basic Properties of HVA

As opposed to the Laplace IVA investigated in the above experiments, HVA does not rely on a theoretical foundation but is heuristically defined by the time-frequency-masking function. Therefore, its performance as well as dependency on the algorithmic parameters must be investigated by experiments. Here, the effects of the parameters in the PDS algorithm (μ_1 , μ_2 and α) and the masking function (λ and σ) were investigated. The other experimental conditions were the same as in the previous subsection.

1) *Effect of the Relaxation Parameter α* : Firstly, the effect of the relaxation parameter α to the performance of HVA was investigated by fixing $\mu_1 = \mu_2 = 1$, $\lambda = 4$, and $\sigma = 0.5$. The results are shown in Fig. 8 (note that the vertical and

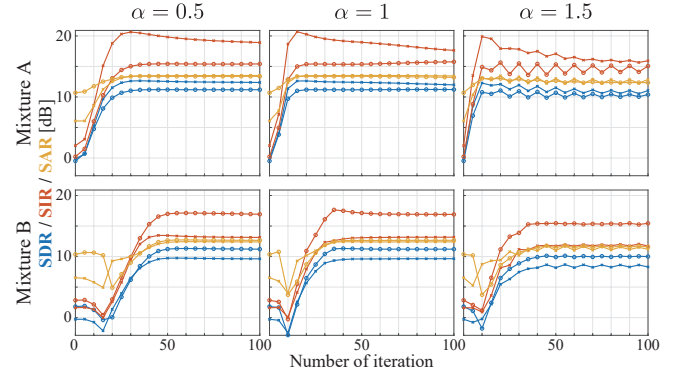


Fig. 8. SDR/SIR/SAR of the separated signals from the mixtures in Fig. 4, where the parameter α was varied (Section VI-B1).

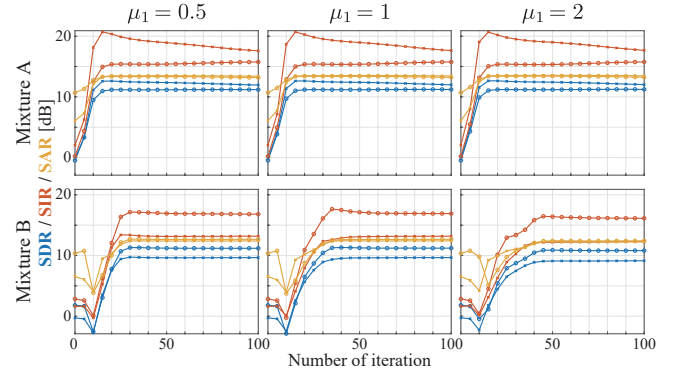


Fig. 9. SDR/SIR/SAR of the separated signals from the mixtures in Fig. 4, where the parameter μ_1 was varied and $\mu_2 = 1/\mu_1$ (Section VI-B2).

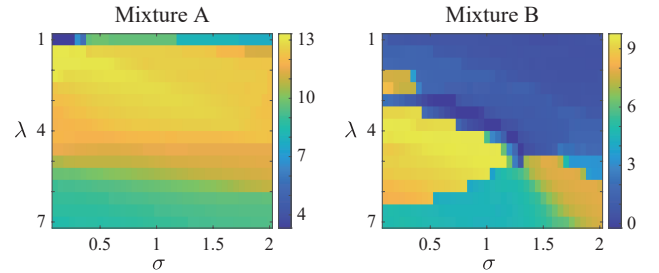


Fig. 10. SDR of the separated signals from the mixtures in Fig. 4, where the parameters of the mask, λ and σ , were varied (Section VI-B3).

horizontal axes are different from those for the Laplace IVA). As the heuristically defined mask may not be stable compared to the proximity operator of the convex function, the choice of the parameter affected the performance at the final iteration. For a masking function that widely varies with iteration, it is expected that smaller α can stabilize the performance because it accumulates the results at each iteration.

2) *Effect of the Step-size Parameters μ_1 and μ_2* : The effect of the step-size parameters μ_1 and μ_2 was also investigated by fixing $\alpha = 1$, $\lambda = 4$, and $\sigma = 0.5$ as in Fig. 9. From the results, it can be seen that the effect of the choice on the step size is not significant compared to the Laplace IVA. This should be because the masking function of HVA in Eq. (47) was defined as the function independent of μ_2 .

3) *Effect of the Thresholding Parameters λ and σ* : The effect of the thresholding parameters, λ and σ , were investigated by fixing $\alpha = \mu_1 = \mu_2 = 1$. The results are illustrated in Fig. 10, which only shows SDR because the other metrics (SIR and SAR) had the same tendency. From the figure, the existence of the regions of success and failure can be confirmed. The thresholding parameters should be the suitable ones for the distribution of the cepstrum coefficients of the observed signals. Investigation of such data-adaptive selection of the parameters is left as a future work.

C. Performance Evaluation of HVA

For evaluating the performance of the proposed HVA, it is compared with the standard method, IVA, and the state-of-the-art method, ILRMA. In this paper, we performed experiments using speech and music mixtures by following the experiments in the popular article proposing ILRMA [18].

1) *Performance Comparison by Speech Signals*: At first, the proposed method was tested by applying it to speech mixtures. The database used in this experiment was a part of SiSEC (the underdetermined audio source separation task) [54]. The BSS methods under test were evaluated for the two cases: 2-channel and 3-channel separation. For the 2-channel signals, 12 speech mixtures (liverec with three sources) contained in dev1 and dev2, which include female/male speech with the reverberation time 130 ms/250 ms and the microphone spacing 1 m/5 cm, were utilized. The first two speech sources for each mixture were chosen to make the task determined ($N = M = 2$) as done in [18]. For the 3-channel signals, 8 speech mixtures in dev3, which include female/male speech with the reverberation time 130 ms/380 ms and the microphone spacing 50 cm/5 cm, were utilized. The first three speech sources for each mixture were chosen to make the task determined ($N = M = 3$). See [54] for the other conditions. The half-overlapping 4096-points-long Hann window (256 ms) was used for STFT as in [18]. All algorithms were iterated 500 times. The number of bases of ILRMA for each source was set to 2 which is suitable for speech signals as shown in [18]. The parameters in Algorithm 4 were set to $\alpha = \mu_1 = \mu_2 = 1$, $\lambda = 4$, and $\sigma = 0.5$. The initial value of the demixing matrices $\mathbf{w}^{[1]}$ was set to the identity matrices ($\mathbf{W}[f] = \mathbf{I}$ for all f), and that of \mathbf{y} was the zero vector.

The experimental results for the 2-channel and 3-channel cases are summarized in Figs. 11 and 12, respectively. From the figures, it can be seen that the proposed HVA outperformed IVA. This result indicates that the harmonic structure can be a useful cue for the separation in determined BSS. Compared to ILRMA, HVA obtained similar results for the 3-channel case. For the 2-channel case, however, HVA outperformed ILRMA on average. While ILRMA utilizes repetition of the spectral pattern with time as a cue for separation, HVA only focuses on the spectral pattern at each time segment independently. As spectral patterns of speech signals widely vary with time, the low-rank structure (or repetitive pattern) of the magnitude spectrogram, assumed in ILRMA, may not effectively serve as a separation cue in this case. In contrast, HVA is not hindered by such variation of signals because HVA considers time-independent information as IVA. Note that, because of such

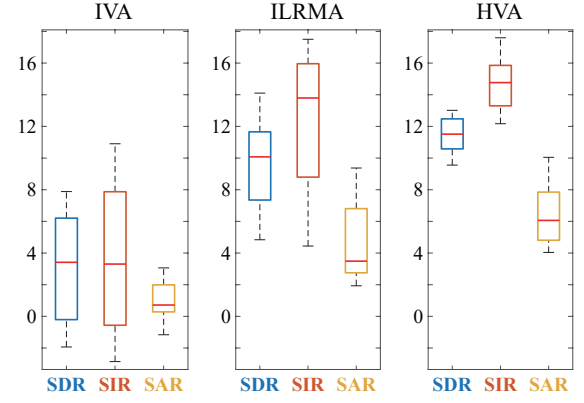


Fig. 11. SDR/SIR/SAR improvements of the separated speech signals from 2-channel mixtures. The experimental settings are explained in Section VI-C1. The central lines indicate the median, and the bottom and top edges of the box indicate the 25th and 75th percentiles, respectively. The vertical axes are expressed in dB.

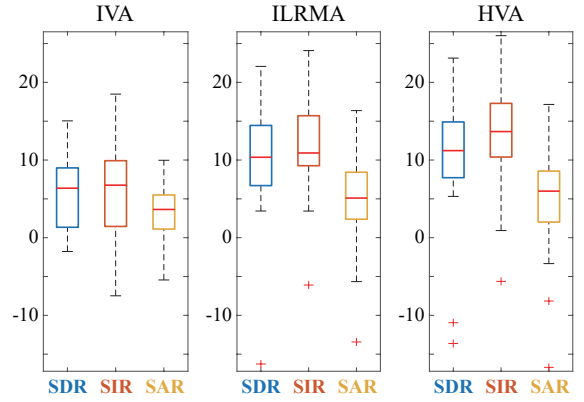


Fig. 12. SDR/SIR/SAR improvements of the separated speech signals from 3-channel mixtures. The experimental settings are explained in Section VI-C1.

time-independent nature, HVA should be more suitable for an online application than ILRMA.

2) *Performance Comparison by Music Signals*: Here, the proposed method was tested by applying it to music mixtures. The database used in this experiment was also a part of SiSEC (the professionally produced music recordings) [54], where the combinations of the source signals utilized in the 2-channel and 3-channel experiments are listed in Tables I and II, respectively. Because *tamy-que_pena_tanto_faz* comprises only two sources (guitar and vocal), it was not included in the 3-channel case. The 2-channel and 3-channel mixtures were produced by convoluting the impulse response E2A or JR2, included in the RWCP database [55], with each source. The recording conditions of these impulse responses are shown in Fig. 13. As in [18], the 3/4-overlapping 8192-points-long Hann window (512 ms) was used for STFT, and the number of bases of ILRMA for each source was set to 30. The other settings of the algorithmic parameters were the same as in the previous experiment using speech signals.

The experimental results for the 2-channel and 3-channel cases are summarized in Figs. 14 and 15, respectively. From

TABLE I
MUSIC SIGNALS FOR THE 2-CHANNEL MIXTURES [54]

Song name	Source (1/2)
bearlin-roads	acoustic_guit_main/vocals
another_dreamer-the_ones_we_love	guitar/vocals
fort_minor-remember_the_name	violins_synth/vocals
ultimate_nz_tour	guitar/synth
tamy-que_pena_tanto_faz	guitar/vocals

TABLE II
MUSIC SIGNALS FOR THE 3-CHANNEL MIXTURES [54]

Song name	Source (1/2/3)
bearlin-roads	acoustic_guit_main/bass/vocals
another_dreamer-the_ones_we_love	drums/guitar/vocals
fort_minor-remember_the_name	drums/violins_synth/vocals
ultimate_nz_tour	guitar/synth/vocals

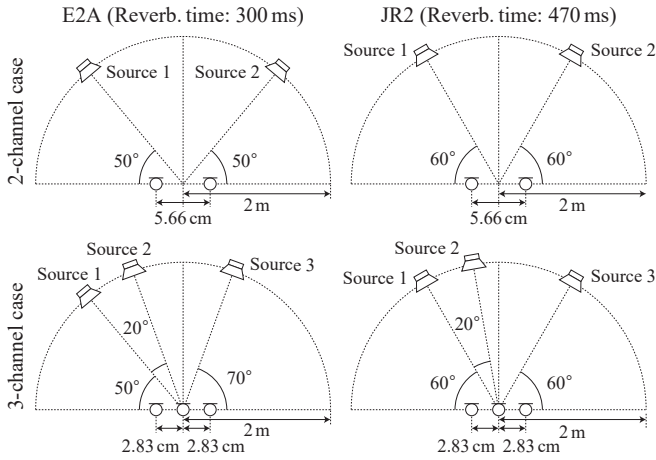


Fig. 13. Recording conditions of the impulse responses (E2A and JR2 [55]) utilized in the experiment in Section VI-C2.

the results of the 2-channel case, it can be seen that the proposed HVA outperformed the other methods. Since the 2-channel mixtures comprise harmonic signals as the sources (see Table I), HVA should have been able to effectively model the harmonic structure through the cepstrum processing. The presence of vocals, whose spectral patterns widely vary, in the four out of five songs might be the favorable situation for HVA as discussed in the previous experiment. In contrast, the performances of the BSS methods under test were almost the same in the 3-channel case. One reason for this result should be the presence of drums in the sources (see Table II) because their dynamic fluctuation with time should be the effective cue for IVA that does not utilize frequency-related information. While ILRMA can handle such percussive sources by devoting some of the bases, HVA does not have a mechanism for explicitly handle them. Note that, as the proposed BSS framework can simultaneously utilize multiple criteria for separation (see Algorithm 3), HVA has a potential of improvement by incorporating other time-frequency masks targeting at the specific structure of the source signals, which is left as a future work.

3) *Computational Effort*: For the experimental conditions in this section, the computational time of HVA was between

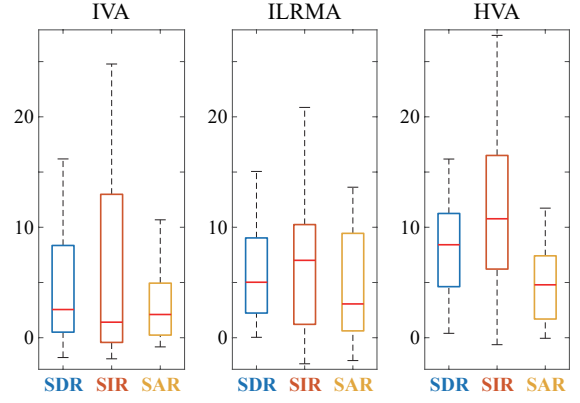


Fig. 14. SDR/SIR/SAR improvements of the separated music signals from 2-channel mixtures. The experimental settings are explained in Section VI-C2.

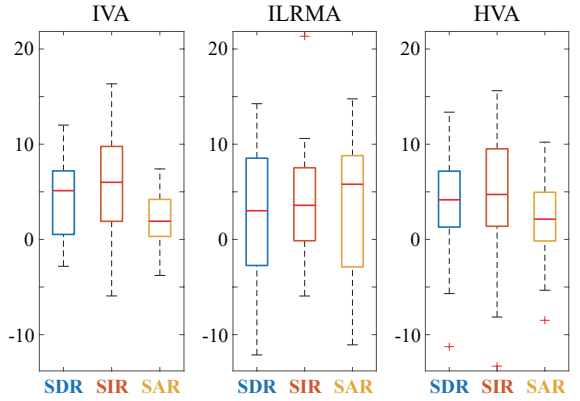


Fig. 15. SDR/SIR/SAR improvements of the separated music signals from 3-channel mixtures. The experimental settings are explained in Section VI-C2.

those of auxIVA and ILRMA. In the experiment using the speech signals, HVA was 1.7 times slower than auxIVA but 1.5 times faster than ILRMA. Similarly in the experiment using the music signals, HVA was 2.1 times slower than auxIVA but 1.4 times faster than ILRMA. Therefore, HVA can be considered as an efficient method that achieves the state-of-the-art performance with less computational cost.

VII. CONCLUSIONS

In this paper, the novel BSS method termed HVA was proposed. By modeling the co-occurrence of the harmonic components via the cepstrum analysis, it achieved the performance comparable to ILRMA with computational effort less than it. To realize HVA, the general BSS algorithm based on time-frequency masking was also proposed by heuristically extending the proximal algorithm. Because the proposed algorithm allows any time-frequency mask for enhancing the source signals, improving HVA as well as investigating a totally new BSS method should be easy. The future works include the extension of HVA by data-adaptive parameter selection, online extension of the proposed algorithm, and investigation of the combination of the proposed algorithm and the existing source enhancement techniques.

REFERENCES

- [1] K. Yatabe and D. Kitamura, "Determined blind source separation via proximal splitting algorithm," in *Proc. IEEE Int. Conf. Acoust., Speech Signal Process.*, Apr. 2018, pp. 776–780.
- [2] K. Yatabe and D. Kitamura, "Time-frequency-masking-based determined BSS with application to sparse IVA," in *Proc. IEEE Int. Conf. Acoust., Speech Signal Process.*, May 2019, pp. 715–719.
- [3] P. Comon, "Independent component analysis, A new concept?" *Signal Process.*, vol. 36, no. 3, pp. 287–314, 1994.
- [4] P. Smaragdis, "Blind separation of convolved mixtures in the frequency domain," *Neurocomputing*, vol. 22, no. 1, pp. 21–34, 1998.
- [5] S. Araki, R. Mukai, S. Makino, T. Nishikawa, and H. Saruwatari, "The fundamental limitation of frequency domain blind source separation for convolutive mixtures of speech," *IEEE Trans. Speech Audio Process.*, vol. 11, no. 2, pp. 109–116, Mar. 2003.
- [6] H. Sawada, R. Mukai, S. Araki, and S. Makino, "Convolutive blind source separation for more than two sources in the frequency domain," in *Proc. IEEE Int. Conf. Acoust., Speech, Signal Process.*, vol. 3, May 2004, pp. 885–888.
- [7] H. Buchner, R. Aichner, and W. Kellermann, "A generalization of blind source separation algorithms for convolutive mixtures based on second-order statistics," *IEEE Trans. Speech Audio Process.*, vol. 13, no. 1, pp. 120–134, Jan. 2005.
- [8] H. Saruwatari, T. Kawamura, T. Nishikawa, A. Lee, and K. Shikano, "Blind source separation based on a fast-convergence algorithm combining ICA and beamforming," *IEEE Trans. Audio, Speech, Lang. Process.*, vol. 14, no. 2, pp. 666–678, Mar. 2006.
- [9] S. Kurita, H. Saruwatari, S. Kajita, K. Takeda, and F. Itakura, "Evaluation of blind signal separation method using directivity pattern under reverberant conditions," in *Proc. IEEE Int. Conf. Acoust., Speech, Signal Process.*, vol. 5, 2000, pp. 3140–3143.
- [10] N. Murata, S. Ikeda, and A. Ziehe, "An approach to blind source separation based on temporal structure of speech signals," *Neurocomputing*, vol. 41, no. 1, pp. 1–24, 2001.
- [11] H. Sawada, R. Mukai, S. Araki, and S. Makino, "A robust and precise method for solving the permutation problem of frequency-domain blind source separation," *IEEE Trans. Speech Audio Process.*, vol. 12, no. 5, pp. 530–538, Sep. 2004.
- [12] H. Sawada, S. Araki, and S. Makino, "Measuring dependence of bin-wise separated signals for permutation alignment in frequency-domain BSS," in *Proc. IEEE Int. Symp. Circuits Syst.*, May 2007, pp. 3247–3250.
- [13] A. Hiroe, "Solution of permutation problem in frequency domain ICA, using multivariate probability density functions," in *Proc. Int. Conf. Independent Compon. Anal. Blind Source Separation*, 2006, pp. 601–608.
- [14] T. Kim, T. Eltoft, and T.-W. Lee, "Independent vector analysis: An extension of ica to multivariate components," in *Proc. Int. Conf. Independent Compon. Anal. Blind Source Separation*, 2006, pp. 165–172.
- [15] T. Kim, H. T. Attias, S. Y. Lee, and T. W. Lee, "Blind source separation exploiting higher-order frequency dependencies," *IEEE Trans. Audio, Speech, Lang. Process.*, vol. 15, no. 1, pp. 70–79, Jan. 2007.
- [16] D. Kitamura, N. Ono, H. Sawada, H. Kameoka, and H. Saruwatari, "Efficient multichannel nonnegative matrix factorization exploiting rank-1 spatial model," in *Proc. IEEE Int. Conf. Acoust., Speech Signal Process.*, Apr. 2015, pp. 276–280.
- [17] —, "Relaxation of rank-1 spatial constraint in overdetermined blind source separation," in *Proc. Eur. Signal Process. Conf.*, Aug. 2015, pp. 1261–1265.
- [18] —, "Determined blind source separation unifying independent vector analysis and nonnegative matrix factorization," *IEEE/ACM Trans. Audio, Speech, Lang. Process.*, vol. 24, no. 9, pp. 1626–1641, Sep. 2016.
- [19] N. Ono and S. Miyabe, "Auxiliary-function-based independent component analysis for super-gaussian sources," in *Proc. Int. Conf. Latent Variable Anal. Signal Separation*, 2010, pp. 165–172.
- [20] N. Ono, "Stable and fast update rules for independent vector analysis based on auxiliary function technique," in *Proc. IEEE Workshop Appl. Signal Process. Audio Acoust.*, Oct. 2011, pp. 189–192.
- [21] K. Lange, *MM Optimization Algorithms*. Philadelphia, PA: Society for Industrial and Applied Mathematics, 2016.
- [22] M. Kowalski, "Sparse regression using mixed norms," *Appl. Comput. Harm. Anal.*, vol. 27, no. 3, pp. 303–324, 2009.
- [23] F. Bach, R. Jenatton, J. Mairal, and G. Obozinski, "Optimization with sparsity-inducing penalties," *Found. Trends Mach. Learn.*, vol. 4, no. 1, pp. 1–106, 2012.
- [24] D. Malioutov and A. Aravkin, "Iterative log thresholding," in *IEEE Int. Conf. Acoust., Speech Signal Process.*, May 2014, pp. 7198–7202.
- [25] R. Chartrand and W. Yin, *Nonconvex Sparse Regularization and Splitting Algorithms*. Cham: Springer International Publishing, 2016, pp. 237–249.
- [26] J. Woodworth and R. Chartrand, "Compressed sensing recovery via nonconvex shrinkage penalties," *Inverse Probl.*, vol. 32, no. 7, p. 075004, 2016.
- [27] I. Bayram and S. Bulek, "A penalty function promoting sparsity within and across groups," *IEEE Trans. Signal Process.*, vol. 65, no. 16, pp. 4238–4251, Aug. 2017.
- [28] P. L. Combettes and J.-C. Pesquet, *Proximal Splitting Methods in Signal Processing*. New York: Springer, 2011, pp. 185–212.
- [29] N. Parikh and S. Boyd, "Proximal algorithms," *Found. Trends Optim.*, vol. 1, no. 3, pp. 127–239, 2014.
- [30] H. H. Bauschke and P. L. Combettes, *Convex Analysis and Monotone Operator Theory in Hilbert Spaces*. Cham: Springer, 2017.
- [31] M. Burger, A. Sawatzky, and G. Steidl, *First Order Algorithms in Variational Image Processing*. Cham: Springer, 2016, pp. 345–407.
- [32] N. Komodakis and J. C. Pesquet, "Playing with duality: An overview of recent primal-dual approaches for solving large-scale optimization problems," *IEEE Signal Process. Mag.*, vol. 32, no. 6, pp. 31–54, Nov. 2015.
- [33] A. Hyvärinen and E. Oja, "Independent component analysis: algorithms and applications," *Neural Netw.*, vol. 13, no. 4, pp. 411–430, 2000.
- [34] A. Hyvärinen, J. Karhunen, and E. Oja, *Independent Component Analysis*, ser. Adaptive and Cognitive Dynamic Systems: Signal Processing, Learning, Communications and Control. Wiley, 2004.
- [35] C. Févotte, N. Bertin, and J.-L. Durrieu, "Nonnegative matrix factorization with the Itakura–Saito divergence. With application to music analysis," *Neural Comput.*, vol. 21, no. 3, pp. 793–830, 2009.
- [36] N. Ono, K. Miyamoto, J. L. Roux, H. Kameoka, and S. Sagayama, "Separation of a monaural audio signal into harmonic/percussive components by complementary diffusion on spectrogram," in *Proc. Eur. Signal Process. Conf.*, 2008.
- [37] P. S. Huang, S. D. Chen, P. Smaragdis, and M. Hasegawa-Johnson, "Singing-voice separation from monaural recordings using robust principal component analysis," in *Proc. Int. Conf. Acoust., Speech, Signal Process.*, 2012, pp. 57–60.
- [38] Y. Ikemiya, K. Itoyama, and K. Yoshii, "Singing voice separation and vocal F0 estimation based on mutual combination of robust principal component analysis and subharmonic summation," *IEEE/ACM Trans. Audio, Speech, Lang. Process.*, vol. 24, no. 11, pp. 2084–2095, Nov. 2016.
- [39] K. Matsuoka, "Minimal distortion principle for blind source separation," in *Proc. SICE Annu. Conf.*, vol. 4, Aug. 2002, pp. 2138–2143 vol.4.
- [40] A. Gramfort, D. Strohmeier, J. Haueisen, M. Hamalainen, and M. Kowalski, "Time-frequency mixed-norm estimates: Sparse m/eeg imaging with non-stationary source activations," *NeuroImage*, vol. 70, pp. 410–422, 2013.
- [41] P. Combettes and J. Pesquet, "Proximal thresholding algorithm for minimization over orthonormal bases," *SIAM J. Optim.*, vol. 18, no. 4, pp. 1351–1376, 2008.
- [42] Y.-L. Yu, "On decomposing the proximal map," in *Adv. Neural Inf. Process. Syst.*, 2013, pp. 91–99.
- [43] N. Pustelnik and L. Condat, "Proximity operator of a sum of functions; application to depth map estimation," *IEEE Signal Process. Lett.*, vol. 24, no. 12, pp. 1827–1831, Dec. 2017.
- [44] M. Kowalski, K. Siedenburg, and M. Dorfler, "Social sparsity! neighborhood systems enrich structured shrinkage operators," *IEEE Trans. Signal Process.*, vol. 61, no. 10, pp. 2498–2511, May 2013.
- [45] R. Chartrand, "Shrinkage mappings and their induced penalty functions," in *IEEE Int. Conf. Acoust., Speech Signal Process.*, May 2014, pp. 1026–1029.
- [46] M. Kowalski, "Thresholding RULES and iterative shrinkage/thresholding algorithm: A convergence study," in *IEEE Int. Conf. Image Process.*, Oct. 2014, pp. 4151–4155.
- [47] I. W. Selesnick and I. Bayram, "Sparse signal estimation by maximally sparse convex optimization," *IEEE Trans. Signal Process.*, vol. 62, no. 5, pp. 1078–1092, March 2014.
- [48] I. Bayram, "Penalty functions derived from monotone mappings," *IEEE Signal Process. Lett.*, vol. 22, no. 3, pp. 265–269, March 2015.
- [49] S. V. Venkatakrishnan, C. A. Bouman, and B. Wohlberg, "Plug-and-Play priors for model based reconstruction," in *IEEE Glob. Conf. Signal Inf. Process.*, Dec. 2013, pp. 945–948.

- [50] A. R. López, N. Ono, U. Remes, K. Palomäki, and M. Kurimo, "Designing multichannel source separation based on single-channel source separation," in *IEEE Int. Conf. Acoust., Speech Signal Process.*, Apr. 2015, pp. 469–473.
- [51] H. Erdogan, J. R. Hershey, S. Watanabe, and J. Le Roux, "Phase-sensitive and recognition-boosted speech separation using deep recurrent neural networks," in *IEEE Int. Conf. Acoust., Speech Signal Process.*, April 2015, pp. 708–712.
- [52] Y. Isik, J. L. Roux, Z. Chen, S. Watanabe, and J. R. Hershey, "Single-channel multi-speaker separation using deep clustering," in *Interspeech 2016*, 2016, pp. 545–549. [Online]. Available: <http://dx.doi.org/10.21437/Interspeech.2016-1176>
- [53] X.-P. Zhang, "Thresholding neural network for adaptive noise reduction," *IEEE Trans. Neural Netw.*, vol. 12, no. 3, pp. 567–584, 2001.
- [54] S. Araki, F. Nesta, E. Vincent, Z. Koldovský, G. Nolte, A. Ziehe, and A. Benichoux, "The 2011 signal separation evaluation campaign (SiSEC2011): - audio source separation -," in *Proc. Int. Conf. Latent Variable Anal. Signal Separation*, 2012, pp. 414–422.
- [55] S. Nakamura, K. Hiyane, F. Asano, T. Nishiura, and T. Yamada, "Acoustical sound database in real environments for sound scene understanding and hands-free speech recognition," in *Proc. Int. Conf. Lang. Resources Evaluation*, 2000, pp. 965–968.

PLACE
PHOTO
HERE

Kohei Yatabe received his B.E., M.E., and Ph.D. degrees from Waseda University in 2012, 2014, and 2017, respectively. He is currently an assistant professor of the Department of Intermedia Art and Science, Waseda University. His research interests include optical measurement of airborne sound.

PLACE
PHOTO
HERE

Daichi Kitamura received the Ph.D. degree from SOKENDAI, Hayama, Japan. He joined The University of Tokyo in 2017 as a Research Associate, and he moved to National Institute of Technology, Kagawa Collage as an Assistant Professor in 2018. His research interests include audio source separation, statistical signal processing, and machine learning. He was the recipient of the Awaya Prize Young Researcher Award from The Acoustical Society of Japan (ASJ) in 2015, Ikushi Prize from Japan Society for the Promotion of Science in 2017, Itakura

Prize Innovative Young Researcher Award from ASJ in 2018, and Young Author Best Paper Award from IEEE Signal Processing Society in 2019.